Noble-gas broadening of the $6\,^2P_{1/2}$-$7\,^2S_{1/2}$ (377.6 nm) $6\,^2P_{3/2}$-$7\,^2S_{1/2}$ (535 nm) thallium lines*

B. Cheron,† R. Scheps,‡ and A. Gallagher§

Joint Institute for Laboratory Astrophysics, National Bureau of Standards and University of Colorado, Boulder, Colorado 80309

(Received 7 September 1976)

The shapes of the thallium (Tl) 535- and 377.6-nm resonance lines broadened by 500–1500 Torr of noble gases have been measured at 743 K. The reported normalized emission intensities yield absorption coefficients in absolute units for all portions of the line. The shift and broadening of the Lorentzian-shaped line cores, the wavelengths of the transition to non-Lorentzian wings, wing shapes, and satellite positions, shapes, and intensities are reported. As an example, a pair of excited and ground-state interaction potentials are given for the Xe case to explain the shift, width, and intensities in all portions of the line wings.

I. INTRODUCTION

The lowest thallium (Tl) atomic levels are represented on Fig. 1. The ground state $6\,^2P_{1/2}$ belongs to the $6s^26p$ configuration. The other component of the doublet ($6\,^2P_{3/2}$) lies 7800 cm^{-1} above the ground state and is metastable. In our experiment Tl atoms are optically excited from the ground state to the $6s^27s$ ($7\,^2S_{1/2}$) state in the presence of noble gases and the shapes of the two subsequent fluorescence lines at 377.6 and 535 nm are studied (hereafter called the uv line and the green line, respectively). The purpose of this work is (1) to measure the shift and broadening coefficents of these two lines due to collisions with noble gases (the impact theory predicts for isolated lines a Lorentzian core of the line with a shift and width that are proportional to the density of perturbers), (2) to determine the approximate wavelength of transition between Lorentzian and non-Lorentzian broadening, and (3) to measure the line-wing intensities in the non-Lorentzian region, including the positions and intensities of the satellites. The present report emphasizes the line core and the spectral regions $|\Delta\lambda| < 10$ nm for each line, where $\Delta\lambda = \lambda - \lambda_0$ and λ_0 is the unperturbed wavelength of the line. In the region $|\Delta\lambda| > 10$ nm the spectrum is highly temperature dependent due to population factors, and as a consequence it can be analyzed using the quasistatic theory to yield the interatomic potentials. This is rather involved and has been reported in another paper.[1]

II. EXPERIMENT AND RESULTS

The reported measurements and analysis are very similar to previously reported measurements of the Rb and Li resonance lines broadened by noble gases,[2,3] so we give only a brief description here.

A cell containing 10^{-7} to 10^{-5} Torr of natural Tl (29.5% ^{203}Tl and 70.5% ^{205}Tl) and up to 1500 Torr of noble gas is illuminated by light from a Tl resonance lamp filtered by an interference filter centered at 377.6 nm. The fluorescence intensity was measured with a 0.75-meter double monochromator equipped with two 2400-grooves/mm holographic gratings, and a cooled GaAs photomultiplier.

As described in Ref. 2 the line shape was obtained by combining scans of different slit width and resolution. This yields line-wing intensities unaffected by instrumental resolution but line-center shapes, typically $|\Delta\lambda| < 0.04$ nm, that are distorted by the instrumental resolution. Measurements were generally made at pressures where the broadened linewidth exceeded the instrumental width, and both greatly exceeded the Doppler width. Then the actual broadening could be accurately determined from comparisons of the measured line-center profiles with theoretical convolutions of Lorentzian lines with the instrument function. This is described in more detail below.

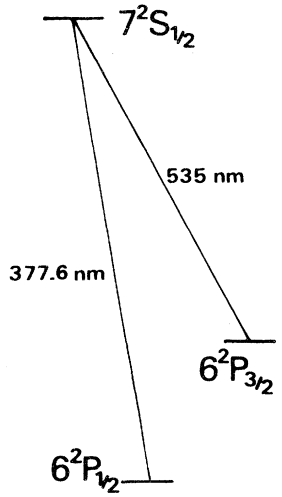

FIG. 1. Lowest three atomic levels of thallium.

The instrument function was determined with an air-cooled low-pressure isotopic mercury lamp (^{198}Hg) using the 365 and 546-nm lines. The resolution was ~0.005 nm at 546 nm and ~0.006 nm at 365 nm for the 12-μ nm spectrometer slit opening used to obtain the line-center data ($|\Delta\lambda| < 0.05$ nm). For the line-center data the output slit position was scanned mechanically to avoid grating-drive irregularities. The accuracy in this scanning was limited by a periodic nonlinearity, with a deviation from linearity of about 4%. The resulting ~4% uncertainty in apparent linewidth made a small contribution to the typical ~10% total uncertainty in the broadening. For $|\Delta\lambda|$ greater than about 0.05 nm, conventional grating driving was used, which did not cause irregularities on the lower resolution scale of the line-wing data.

The fluorescence intensities are reported as normalized emission coefficients $I(k)/N\int I(k)\,dk$ for each line, where $I(k)$ is the fluorescence intensity per wave number, $k = 1/\lambda$, $k_0 = 1/\lambda_0$, $\Delta k = k - k_0$, N is the noble gas density and the integral is over one line from $k_0 - W$ to $k_0 + W$, where $W \cong 50$ cm^{-1}. For the pressures in our experiment this emission coefficient is independent of the Tl and noble-gas densities for wavelengths outside the Lorentzian-core region (indicating that binary interactions with the perturber rather than three-body collisions are dominant). This emission coefficient is related to the absorption coefficient by simple thermodynamic factors equivalent to the Einstein A-B relations.[3]

Since radiative trapping attenuates the center of a line, thereby yielding erroneous normalized wing intensities [due to inaccuracy of $\int I(k)\,dk$], it is necessary to measure these emission coefficients from optically thin Tl vapor, or in the limit of zero Tl density. This Tl experiment is particularly simple in this regard as the $6^2P_{3/2}$ metastable state is very slightly populated thermally and the $7^2S_{1/2}$-$6^2P_{3/2}$ (green) line should not be radiatively trapped since, as explained later, the $6^2P_{3/2}$ state is not optically pumped. Thus the green line shape can be measured at relatively high Tl densities (~10^{-5} Torr), providing larger signals. Furthermore, if the ratio R of the uv to green-line total intensities is measured once in the absence of radiation trapping ($R = R_0$), this can be used to correctly normalize uv line-wing data taken in the presence of radiation trapping in the center of the uv line. In the present experiments the light intensity was low enough and the $6P_{3/2}$ state quenching rate due to molecular impurities (probably ~10^{-1} Torr in 10^3-Torr noble gas) high enough, so that insignificant optical pumping of the $6^2P_{3/2}$ state occurred. This was confirmed by the fact that the ratio R was not affected by lowering the intensity of the excitation lamp. Then R was measured in the limit of zero Tl density to obtain R_0, and all the line-wing data were normalized to the green line. During the line-shape measurements R was typically 10% lower than R_0. The shape of the uv line core was measured at relatively lower Tl densities (estimated ~10^{-6} Torr), where typically ~3% attenuation of the line peak occurred. This causes a few percent apparent broadening, but was deemed too small to warrant a correction.

The emission coefficients for perturber pressures between 500 and 1500 Torr are given in Fig. 2 for the uv line and in Fig. 3 for the green line. These spectra represent the actual fluorescence intensity distribution, essentially unaffected by instrument resolution, for $|\Delta\lambda| > 0.05$ nm. The solid lines in Figs. 4 and 5 represent the measured emission coefficients in the line-core region for the uv and the green lines, respectively, for various pressures. These spectra are influenced by the instrumental resolution. The experimental results are compared to theoretical convolutions of the instrument function with the Lorentzian-broadened components corresponding to the thal-

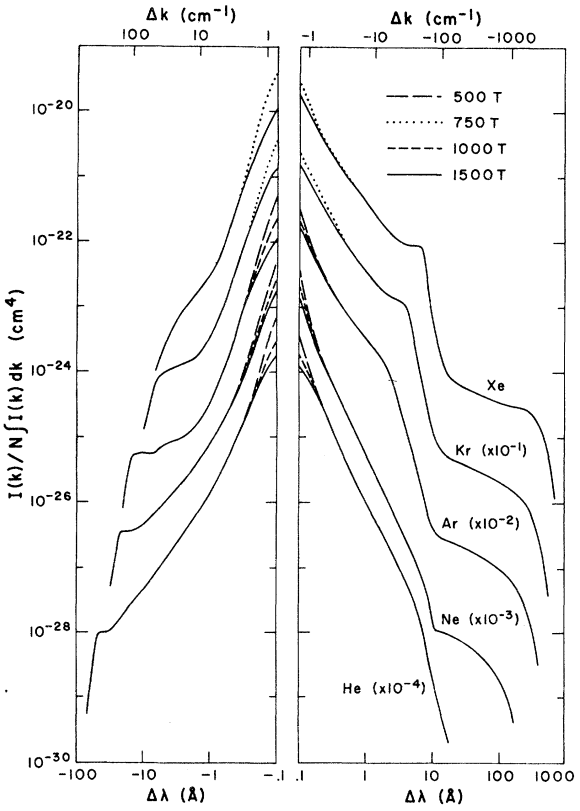

FIG. 2. Normalized emission intensities of the Tl 377.6-nm line broadened by the noble gases at the cell temperature of 743 K.

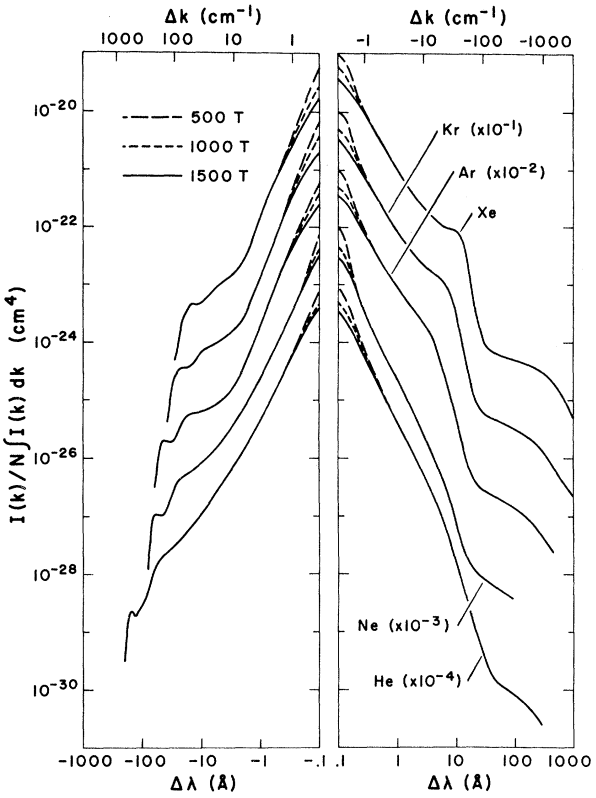

FIG. 3. Same as Fig. 2 for the Tl 535-nm line.

lium hyperfine structure.[4] As the isotope shift is minor, only hyperfine components, shown in Figs. 4 and 5, were used. The Doppler contribution to the line shape is very minor and is partly included in the instrument function. The same Lorentzian parameters γ and Δ in $I \propto [(\frac{1}{2}\gamma)^2 + (\Delta k - \Delta)^2]^{-1}$ are used for each component. The relative intensity of the different components would be statistical for white-light excitation or complete collisional mixing, but the lamp spectrum is less at the weaker (smaller F) components and the $7\,^2S_{1/2}$ state is not easily depolarized by noble-gas collisions. Thus the hyperfine component intensities arising from the smaller $7\,^2S$ state F components had to be decreased about 20% from statistical to fit the experimental spectra. The convolutions are calculated with $\Delta = 0$ and then shifted to yield optimum visual fits in the line-core region. The γ parameters are chosen to optimize the fits in the line-core region where the lines appear to be nearly Lorentzian. The comparisons are shown in Figs. 4 and 5. It can be seen that except for He (uv and green lines) and Ne (uv line), a good fit to the Lorentzian convolution is obtained in the line-core region. The misfit for the He and Ne cases is not severe, and

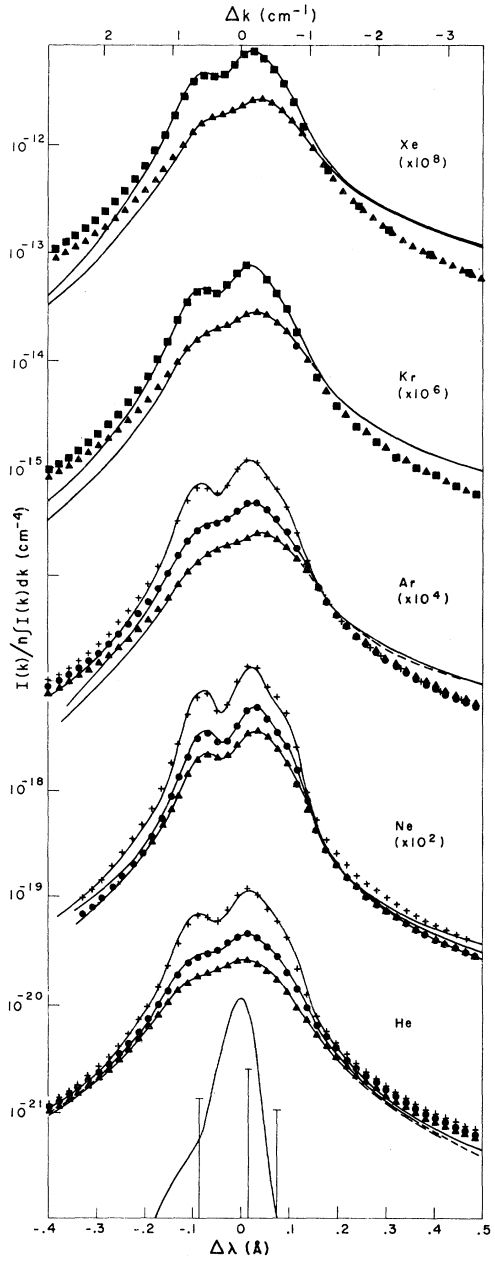

FIG. 4. Measured normalized emission intensities (full lines) in the central region of the Tl 377.6-nm line. For He, Ne, and Ar, the upper line is for 500-Torr perturber pressure, the middle for 1000 Torr and the lower for 1500 Torr. For Kr and Xe the upper line is for 750 Torr and the lower for 1500 Torr. The hyperfine structure and the instrument profile (~0.4-cm^{-1} resolution) are indicated at the bottom of the figure. Theoretical convolutions of the instrument function with Lorentzian-shaped line components are given as variously shaped +, Δ, and ○ points. The shift and Lorentz width parameters used in these convolutions are given in Figs. 6 and 7.

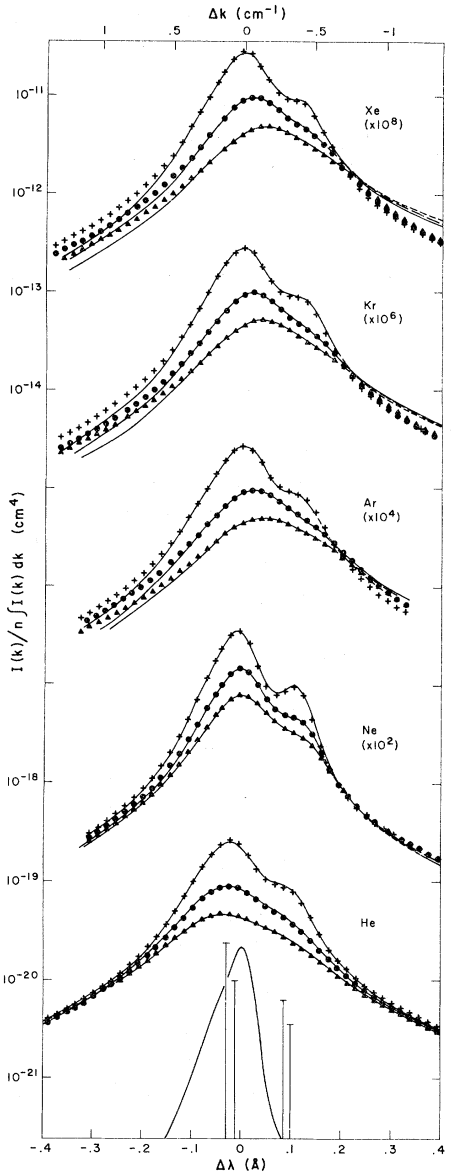

FIG. 5. Same as Fig. 4 for the Tl 535-nm line except that for each perturber case the upper line is for 500 Torr, the middle for 1000 Torr and the lower for 1500 Torr.

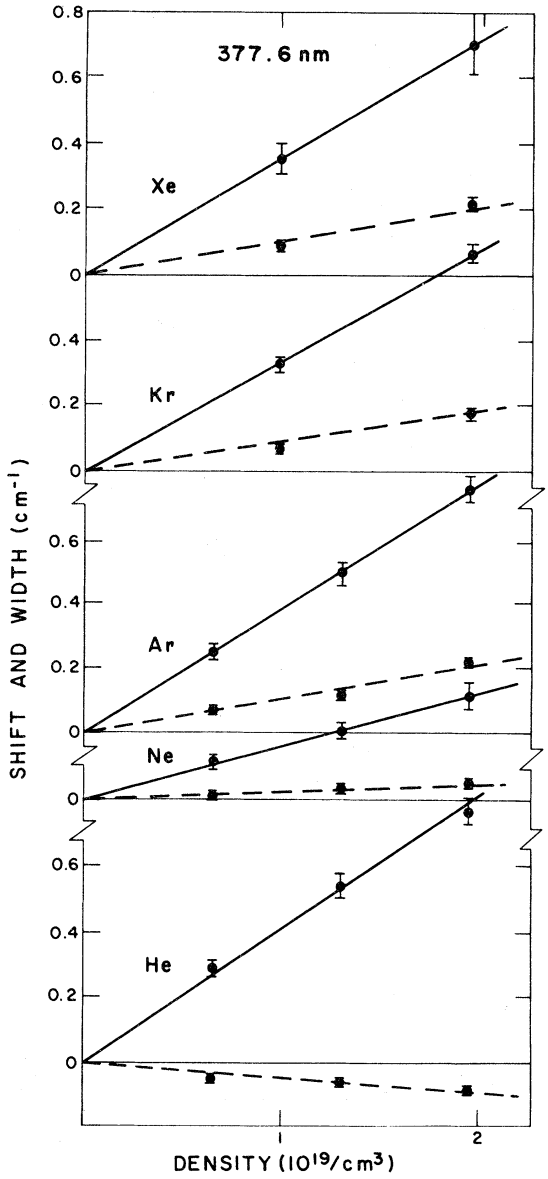

FIG. 6. Shifts Δ (dashed lines) and full Lorentz widths γ (solid lines) of the 377.6-nm line obtained from Fig. 4.

is attributed primarily to instrumental effects.

The shift (Δ) and full width (γ) of the Lorentzian portion of the lines are plotted versus density of perturber in Fig. 6 for the uv line and Fig. 7 for the green line. The slopes of the fitted lines in Figs. 6 and 7 are reported as shift and broadening rates in Table I. Also included in this table is the estimated value of the wavelength of the transition between Lorentzian and non-Lorentzian broadening from the convolution fitting in Figs. 4 and 5. This transition point is the estimated point of departure of the actual wing *slope* from that predicted by the Lorentzian convolution. In Table II, we give the effective power dependence n, in $I \propto |k - k_0 - \Delta|^{-n}$, of the wing intensities in these non-Lorentzian regions adjacent to the Lorentzian core (see Figs. 2 and 3). The fitted wavelength range is also given. This is not intended to imply actual power-law intensity dependences; rather there is a region on each wing where a power law gives a good fit across 1–2 decades in intensity.

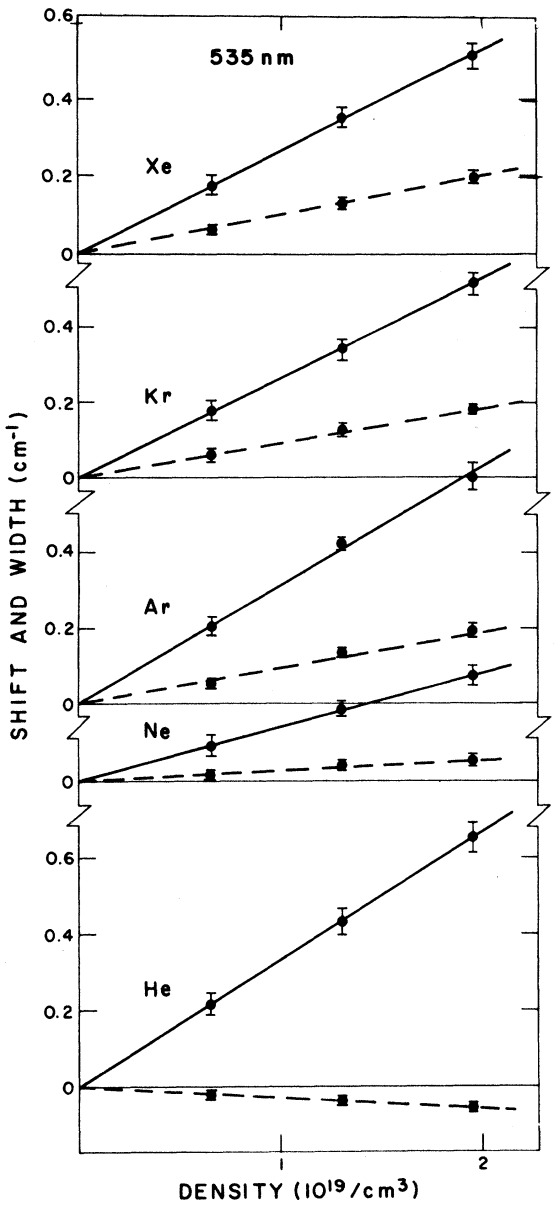

FIG. 7. Shifts Δ (dashed lines) and full Lorentz widths γ (solid lines) of the 535-nm line obtained from Fig. 5.

The fit typically determines n with about ±5% accuracy. Finally, we give in Table III the estimated position of the centers of the satellites in Figs. 2 and 3 and compare with other data. In many cases these satellites are so broadened that they are mere inflections whose centers are ill defined.

III. INTERATOMIC POTENTIALS FROM THE DATA

The far wings of these broadened Tl lines are due to close-range Tl–noble-gas interactions. They can be analyzed with the use of the quasistatic theory to yield information about the interatomic potentials at internuclear separations R of typically 3–4 Å The satellites, attributed to extrema in the difference potential $\Delta V(R) = V^*(R) - V(R)$ in the 4–8-Å regions, yield information about these portions of the potentials. The intensities in the wings adjacent to the Lorentzian core of the lines yield information on the 8–12-Å parts of the potentials. Finally, the broadening and shift are related to the potentials in the region of the Weisskopf radius, typically 12–20 Å. C_6 coefficients based on isolated atomic properties also yield potentials in these large-R regions. Thus when absolute intensity information is available in all these portions of the line it provides a very powerful tool for determining the interatomic potentials $V^*(R)$ and $V(R)$ for the upper and lower states of the transition. The inversion of the data to yield these potentials is almost unique in the small-R regions where $[V^*(R) - V^*(\infty)]/kT \geq 1$, since thermal population (Boltzmann) factors yield large temperature dependences that depend on the potentials[1]. The inversion of the data in other portions of the line to yield $V^*(R)$ and $V(R)$ is much less unique. Nonetheless, we will demonstrate that this inversion can sometimes be done with surprisingly little ambiguity, and we give here an example. This analysis is much simpler if the atomic interactions produce only a single $V^*(R)$ and $V(R)$; so we choose the Tl $7\,^2S_{1/2}$–$6\,^2P_{1/2}$ (uv) line for the example as it satisfies this criterion. [The Tl ($6\,^2P_{3/2}$) state splits into two $V(R)$ and must be analyzed in terms of superpositions of bands.] We will describe the Tl-Xe case in detail, since the other cases can be generalized from this with very minor changes.

The analysis of the temperature-dependent far-wing intensities ($\Delta\lambda > 15$ Å in Fig. 2) to yield $V^*(R)$ and $V(R)$ in the 3–4-Å region have already been described in Ref. 1 and will not be repeated here. These $V^*(R)$ and $V(R)$ are shown for the Tl-Xe case considered here in Fig. 8. We will now extend that analysis to the remaining, larger-R regions. We will assume a familiarity with the quasistatic theory as described in Ref. 1 and references cited therein. For the more polarizable noble-gas cases (Ar, Kr, and Xe) we expect $V^*(R)$ to be more attractive at long range than $V(R)$, since the excited-state wave function is much larger and more polarizable, i.e., $C_6^* > C_6$ in $V^*(R) - V^*(\infty) = C_6^* R^{-6}$ and $V(R) - V(\infty) = C_6 R^{-6}$. This is also required to explain the large red-wing intensities for these cases (Fig. 2). Thus $\Delta V(R) - \Delta V(\infty)$ must be negative at large R ($R > 8$ Å in Fig. 8) and approach zero with a positive slope as $R \to \infty$.

TABLE I. Shift Δ and full width γ of the Lorentzian line core.[a]

Line	Perturber	Δ/N (cm^{-1}/r.d.)	γ/N (cm^{-1}/r.d.)	$k-k_0$ at non-Lorentzian[b] transition zone (cm^{-1})	
377.6 nm	He	$+0.13\pm0.03$[c]	1.06 ± 0.1	+7	−28
	Ne	-0.070 ± 0.02	0.44 ± 0.05	...[d]	−14
	Ar	-0.27 ± 0.04	1.01 ± 0.06	+1.0	−1.2
	Kr	-0.23 ± 0.05	0.91 ± 0.07	+1.0	−1.0
	Xe	-0.27 ± 0.05	0.98 ± 0.1	+0.85	−1.0
535 nm	He	$+0.065\pm0.015$	0.91 ± 0.06	+9	−12
	Ne	-0.085 ± 0.02	0.40 ± 0.04	...[d]	−7
	Ar	-0.27 ± 0.02	0.84 ± 0.06	+0.4	−0.7
	Kr	-0.25 ± 0.02	0.72 ± 0.04	+0.4	−0.7
	Xe	-0.28 ± 0.02	0.72 ± 0.02	+0.4	−0.7

[a]The shift and broadening coefficients are given per r.d. or relative density where 1 r.d. $=2.69\times10^{19}$ cm^{-3} is the density of the perfect gas at standard temperature and pressure. The values are given at $T=743\pm5$ K except for 377.6 nm (He, Ne, Ar) and 535 nm (Ar) where $T=720\pm5$ K.

[b]Due to the large hyperfine structure, the magnitude of the values indicated for Ar, Kr, Xe are upper limits.

[c]The uncertainties represent ± one standard deviation of statistical and estimated systematic effects.

[d]The transition could not be determined due to the small change in wing power dependence (see Table III).

The intense red wing in the $\Delta\lambda=1-10$ Å portion of the Tl-Xe spectrum in Fig. 2 terminates in a red "satellite" or shoulder whose outer edge is at ~−50 cm^{-1}. Thus $\Delta V(R)$ must reach a negative extremum of $\Delta V\cong-50$ cm^{-1} and then reverse slope (~6 Å in Fig. 8). This red shoulder might also have been attributed to merely a flattening of $\Delta V(R)$ in the 6-Å region, followed by an increasingly negative ΔV ($R<6$ Å). However, there is a severely broadened shoulder or "satellite" on the Tl-Xe blue wing in Fig. 2, which requires that $\Delta V(R)$ must have a positive maximum at some R. From the general satellite-shape theory of Sando and Wormhandt[8] we attribute this to a maximum of about +30 cm^{-1} in ΔV; a $|\Delta k|$ slightly past the shoulder where the intensity is beginning to drop more rapidly. The only R region where this positive $\Delta V(R)$ can occur at is between the large R and small R regions of negative $\Delta V(R)$. This occurs very naturally at ~4.5 Å in Fig. 8 by a smooth extension of $\Delta V(R)$ at small R and attributing the red satellite to an actual minimum, not an inflection, at ~6 Å. Thus, while this result is nonunique, we believe that no other reasonable form for $\Delta V(R)$ could explain the data; it must be negative at small and large R with a positive extremum in between, as given in Fig. 8.

The R scale in Fig. 8 has been determined using

TABLE II. Wing power dependence ($I\sim|k-k_0-\Delta|^{-n}$).

Line	Perturber	Blue wing n	Blue wing $\lvert k-k_0\rvert$ Range (cm^{-1})	Red wing n	Red wing $\lvert k-k_0\rvert$ Range (cm^{-1})
377.6 nm	He	2.1	2.5–7	2.0	0–30
	Ne	2.3	2–5.5	2.0	0–15
	Ar	3.8	2.5–4.5	1.4	3–10
range	Kr	3.2	2.5–5	1.3	3.5–9
	Xe	3.2	2.8–5	1.3	3.5–15
535 nm	He	2.0	0–7	2.0	0–12
	Ne	2.2	1–5	2.0	0–7
	Ar	2.7	1.2–7	1.5	1–10
	Kr	2.7	1.2–5	1.6	1–3.5
	Xe	2.8	1–5	1.7	1.5–7

TABLE III. Satellite positions.

Line	Perturber	Present (T=743 K) $\Delta\lambda$ (nm)	Present (T=743 K) Δk (cm^{-1})	Other experiments Δk (cm^{-1})	Other experiments T (K)
377.6 nm	He	−4.4±0.3	309±21	314±14[b]	973
	Ne	−2.0±0.1	140±14	144±10[b]	973
	Ar	+0.2±0.05[a]	−14±3.5	82±7[b]	823
		−13±1	91±7		
	Kr	+0.37±0.03	−26±2	−24.6±2.0[b]	798
		−0.55±0.05	38.5±3.5	35.1±7[b]	1393
	Xe	+0.68±0.03	−48±2	−41.5±35[b]	798
		−0.5±0.1[a]	35±7		
535 nm	He	−5.0±0.3[a]	175±11	576[c]	
		−14.5±0.2	507±7		
	Ne	−1.5±0.3[a]	52±11		
		−6.0±0.5	210±18	249[c]	
	Ar	+0.37±0.05[a]	−13±2		
		−1.7±0.2	59.5±7		
		−4.5±0.2	157±7	173[c]	
	Kr	+0.6±0.1[a]	−21±3.5		
		−1.0±0.1[a]	35±3.5		
		−2.4±0.2	84±7		
	Xe	+1.0±0.1	−35±3.5		
		−1.5±0.1	52.5±3.5		

[a] Broad satellites. [b] Reference 5. [c] Reference 6.

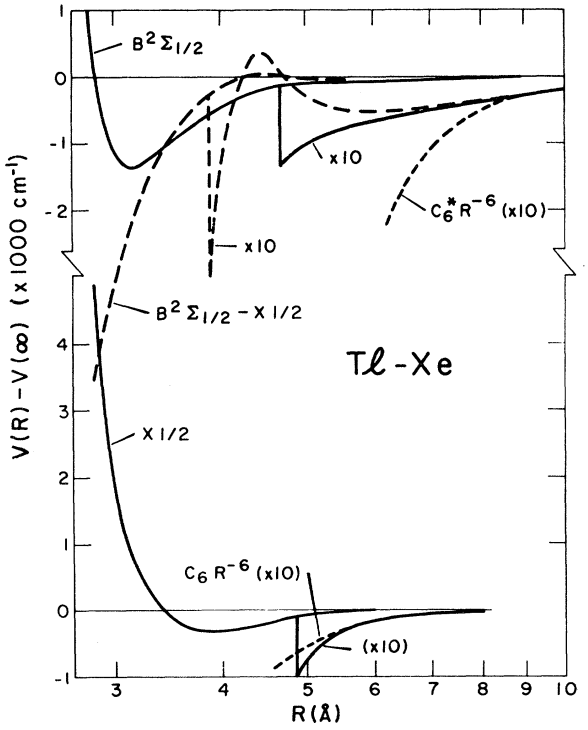

FIG. 8. Tl-Xe interatomic potentials associated with the 377.6-nm line. The $B\,^2\Sigma_{1/2}$ state connects to the Tl ($7\,^2S_{1/2}$) state and the $X\frac{1}{2}$ to the Tl ($6\,^2P_{1/2}$) state at large R. (See Ref. 1 for the explanation of the nomenclature for the molecular states.) The region $R<4$ Å is from the analysis of Ref. 1, $C_0^*=2800$ and $C_6=160$ a.u.

the measured normalized intensities and the assumption of a transition moment independent of R in the quasistatic theory, as explained in Ref. 1 for the far wing data. Thus, for example, the differential volume $\int_{R_1}^{R_2} 4\pi R^2\,dR$ in which $\Delta V(R)$ exceeds +15 cm^{-1} in Fig. 8 (~4.3–4.6 Å) must equal the area $\int_{k_1}^{k_2} I_N(k)\,dk$ under the measured spectrum of Fig. 2 from $k_1=+15$ to $k_2=+40$ cm^{-1}, which is due to the blue satellite. (Note that $\int dk$ of the normalized intensity in the cm^4 units of Fig. 2 has units of cm^3.) As another example, the differential volume from 5.0–10.0 Å in Fig. 8, where $\Delta V(R)<-20$ cm^{-1}, agrees with the integrated intensity from −20 to −70 cm^{-1} in Fig. 2. By thus using a large $-\Delta k$ region about the satellite the exact details of the satellite shape are not necessary to obtain the R scale. The severely smeared-out form of the blue satellite may be understood as due to the breakdown of the quasistatic approximation once the R scale is obtained in Fig. 8, because the positive $\Delta V(R)$ region is seen to be very narrow and will be traversed rapidly using a collision orbit or bound molecular vibration.

The shift and width of the line core are determined predominantly by $\Delta V(R)$ in the region of the Weisskopf radius R_W, given by the impact parameter where the phase shift $\int dt\,\Delta V[R(t)]/\hbar=1$. For a $\Delta V=C_6^e R^{-6}$, $R_W=(3\pi C_6^e/8\hbar\langle v\rangle)^{1/5}\cong 19$ Å in the present case. The effective $C_6^e=C_6^*-C_6$ obtained from equating the measured broadening rate to

that[9] for $\Delta V = C_6^e R^{-6}$ is much larger than C_6; so it can be used to establish a C_6^*. This $C_6^* R^{-6}$ long-range form for $V^*(R)$ is shown in Fig. 8, where it can be seen to blend at large R with the $V^*(R)$ obtained from the above analysis of the wing intensities. The approximately $\Delta k^{-1.3}$ behavior at 4–15 cm^{-1} on the Tl-Xe red wing (Table II) is consistent with a slightly more gradual change in $V^*(R)$ as compared to C_6^*/R^6 for $R > 10$ Å, as implied by the less attractive $V^*(R)$ shown for $R < 10$ Å. The red-shift to width ratio[10] for a $\Delta V(R) = C_n R^{-n}$ is $|\Delta/\gamma| = 0.36$ for $n = 6$, increasing to 0.85 for $n = 4$. We observe ratios of 0.5–0.7 for the Ar, Kr, and Xe perturber cases, which also implies more gradual decreases in $V^*(R)$ at large R compared to $C_6^* R^{-6}$ interaction.

Once $\Delta V(R)$ is established, it is still desirable to obtain $V^*(R)$ and $V(R)$. As noted above, the analysis of the temperature-dependent extreme wings in Ref. 1 fixed $V^*(R)$ and $V(R)$ for $R = 2.8$–0.4 Å in Fig. 8. The C_6 coefficient for the ground state can be estimated fairly reliably, as discussed in the next section, and this yields the $R > 5$ Å portion of $V(R)$ in Fig. 8. The $V(R)$ shown has simply been connected smoothly between 4.0 and 5 Å. Adding this $V(R)$ to $\Delta V(R)$ then yields the $V^*(R)$ in Fig. 8. At $R > 8$ Å, $\Delta V \cong V^*$ and the data yield V^* directly. It is satisfying that the $V(R)$ and $V^*(R)$ which result have typical, simple shapes with a single minimum and a single inflection. Only the relatively flat, extended portion of V^* for $R > 5$ Å is at all unusual.

It is apparent from Fig. 2 that the Tl-Kr, Ar, Ne uv lines can be similarly analyzed. For the Ar and Kr cases the shape of $\Delta V(R)$ will be very similar to Tl-Xe. The $|\Delta k|$ at the minima and maxima of $\Delta V(R)$ will change to accomodate the different satellite positions, with the general trend that $\Delta V(R)$ attains a larger positive value and is positive over a larger-R range for lighter perturbers. The Δk and R range associated with the red satellites decrease with the lighter perturbers, until for He and Ne the long-range $\Delta V(R)$ probably becomes positive. The only feature in Fig. 2 which does not fit this consistent picture is the double hump at the Tl-Ar blue satellite, which might be due to a double inflection in ΔV ($R \sim 5$ Å) or an interference effect as observed in Ref. 7.

As noted above, the green line is due to two $V(R)$ which connect to the Tl $6^2P_{3/2}$ state. In spite of overlapping of the two $\Delta V(R)$ bands the temperature-dependent extreme red wings and blue satellites of this line could be analyzed in Ref. 1 to yield both of these $V(R)$ in the 3–5-Å regions, starting with a $V^*(R)$ obtained from the uv line analysis. [Each of the two "satellites" on the blue wings in Fig. 3 is attributed to one of the $V(R)$ in the 4–5-Å region.] These $V(R)$ connect to the two ($|M| = \frac{3}{2}, \frac{1}{2}$) states arising from $^2P_{3/2}$, so the known $|M|$ dependence of the dipole-dipole interaction combined with the near red wing intensity and satellites allows for fairly good estimates for these $V(R)$ at $R > 5$ Å, at least for the Ar, Kr, and Xe cases. However, a detailed example of this does not appear appropriate at this time.

IV. DISCUSSION OF THE LINE CORE

The line-center measurements (Figs. 4 and 5) show a departure from Lorentzian shape very near the line core for Ar, Kr, and Xe perturbers. As this occurs almost within the hfs splitting, the convolution fitting analysis is somewhat uncertain. Despite this fact, the shift and Lorentzian broadening coefficients obtained from the line core fitting in Figs. 4 and 5 are linear with pressure (Figs. 6 and 7), and this uncertainty is considered to be included in the values given in Table I. The red-shift rates are approximately the same for the three heavier gases, smaller for Ne, and for He we notice a small blue shift for both lines. The broadening rates are similar for He, Ar, Kr, and Xe and smaller for Ne. This is typical behavior for many species, and can be given a similar qualitative explanation (e.g., Refs. 2 and 3). Departure from Lorentzian shape does not appear within the range of our high-resolution scans for the green line perturbed by He and Ne (Fig. 5), which is consistent with the Lorentzian power dependence observed to $|\Delta k| \geq 5$ cm^{-1} in the low-resolution scans (Fig. 3 and Table II). But for the uv line perturbed by He and Ne the theoretical convolutions do not fit the data in some portions of the wings (Fig. 4). The power-law dependences on these wings, as observed in the lower-resolution scans, are very nearly Lorentzian to $|\Delta k| \sim 6$ cm^{-1} (Fig. 2 and Table II) as roughly expected due to the higher collision velocities and close-range impacts for He and Ne. Thus the discrepancies in Fig. 4 are attributed to experimental problems. The most likely candidate is drift in the spectrometer slit width with a resultant drift in the shape of the instrument function. As the instrument function is highly asymmetric for the uv line (Fig. 4) this would most severely affect the more rapidly dropping red wings of the He and Ne broadened uv line. As the values of γ for the uv line broadened by He and Ne could be inferred from the low-intensity data out to ~ -6 cm^{-1} as well as from the $|\Delta k| < 1.5$ cm^{-1} portions of the high-resolution data this did not hurt the final accuracy.

The impact approximation predicts a Lorentzian line core for any form of ΔV. It is interesting to compare the wing intensity dependences just out-

side this line core with theoretical predictions for $\Delta V = -C_6^e R^{-6}$, to see if this is a reasonable approximation for the appropriate larger R range. Only Ar, Kr, and Xe have sufficient polarizability to make this comparison meaningful; so we will only consider those cases. The theory[10,11] predicts a $\Delta k^{-3/2}$ quasistatic profile on the red wing [e.g., Eq. (8.6) of Ref. 10], and a $\Delta k^{-3/2}\exp(-K\Delta k^{5/9})$ dependence on the blue wing [e.g., Eq. (8.10) of Ref. 10, where K is a constant related to C_6^e and the average collision velocity]. This blue-wing line shape results from averaging over a kinetic velocity distribution the single-velocity result $\Delta k^{-7/3}\exp(-K'\Delta k^{5/6})$, as was obtained in Refs. 12 and 13. For noble-gas perturbers, the C_6 coefficients are proportional to

$$\alpha \sum_j f_{ij}(E_j - E_i)^{-1},$$

where α is the noble-gas polarizability, and f_{ij} and E_i are the Tl oscillator strengths and energies. Sufficient oscillator strengths are known from the $6\,^2P_J$ state to estimate these C_6 coefficients with about 30% accuracy, but the oscillator strengths which determine the dominant C_6^* for the $7\,^2S_{1/2}$ state are much less certain. However, Ref. 14 provides an approximation for C_6^* based on the binding energy of the $7\,^2S_{1/2}$ state. If we assume the measured broadening of the Lorentzian core of the line is due to a $\Delta V = -C_6^3 R^{-6}$, we can also obtain a "measured" C_6^e and thereby a "measured" C_6^* from Eq. (4.19) of Ref. 10. The resulting "measured" C_6^* for Ar, Kr, and Xe perturbers are given in Table IV, where they are compared to the values calculated according to Ref. 14. The agreement in magnitude is good. However, the C_6^* obtained from the green and uv line broadenings for each gas differ considerably, and these C_6^* are not proportional to noble-gas polarizabilities as they should be. Using these "measured" C_6^e in the static wing (8.6) and antistatic wing (8.10) equations of Ref. 10, the theoretical line wings in Fig. 9 are also obtained. The experimental results can be seen to compare moderately well with these on each wing until the satellite regions are approached. Since we have fixed C_6^e to obtain $\gamma_{\text{theor}} = \gamma_{\text{expt}}$ the data converge to the Lorentzian line-core theory in the $|\Delta k| < 1$ cm^{-1} region not shown in Fig. 9. Most of the discrepancies in the wings can be attributed to departure of $\Delta V(R)$ from the $C_6^e R^{-6}$ form and quasistatic contributions to the blue wings from the positive $\Delta V(R)$ regions at smaller R (e.g., 4.5 Å in Fig. 8). The magnitude of this departure is reasonable since the $C_8 R^{-8}$ energy for Tl $7\,^2S_{1/2}$ + Xe, using C_8 from Ref. 14, yields about a 10% increase in $|(d/dR)\Delta V(R)|$ in the $R \sim 20$ Å region responsible

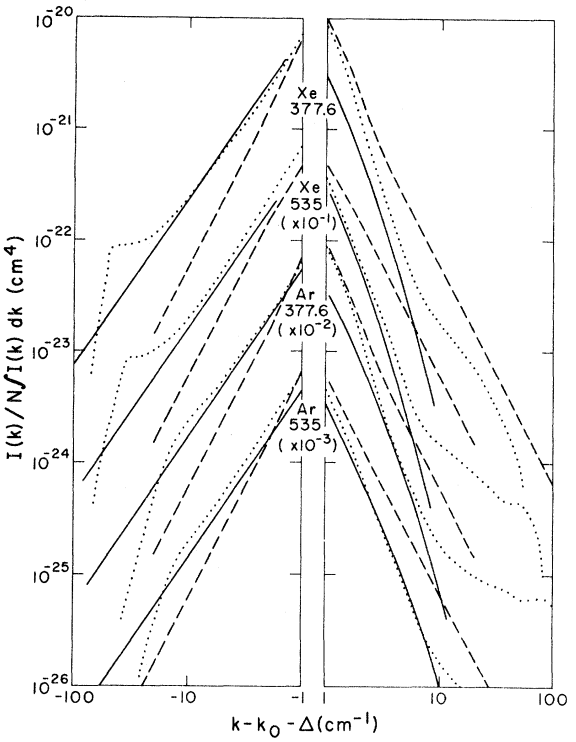

FIG. 9. Comparison of theoretical (solid line) and near-wing intensities, for $\Delta V(R) = -C_6^e R^{-6}$ with C_6^e obtained from Lorentzian linewidths, to experimental intensities (points). The Lorentzian line-core shape, convoluted with hfs and instrument function, has been extended to larger $|\Delta k|$ to show the difference between the theoretical and Lorentzian wings (dashed lines). The effect of the instrument function and hfs can be seen as minor departures of the latter from straight lines in the $|\Delta k| < 2$ regions. The static (red) wing is to the left of the figure.

TABLE IV. Tl–noble-gas C_6 coefficients.[a]

Tl state	Ar	Kr	Xe
$6\,^2P_{1/2}$[b]	65	100	160
$6\,^2P_{3/2}$[b]	105	190	300
$7\,^2S_{1/2}$ (535)[c]	1050	1150	1500
$7\,^2S_{1/2}$ (377.6)[c]	1500	1900	2800
$7\,^2S_{1/2}$[d]	650	970	1560

[a] The C_6 coefficients in $V(R) - V(\infty) = -C_6 R^{-6}$, are in atomic units ($e^2 a_0^5$).

[b] C_6 coefficients estimated from known oscillator strengths and sum rules. The $6\,^2P_{3/2}$ case is $|m|$ averaged.

[c] From measured broadening rates.

[d] From Ref. 14.

for the line-core data. The experimental spectra indicate a *decrease* of comparable magnitude. It is important to note that both the experimental and theoretical intensities are in the same absolute units; the only adjustable parameter in the comparisons of Fig. 9 is C_6^e, which has been chosen to yield the measured broadening. Since the theoretical broadening[10] is proportional to $(C_6^e)^{0.4}$ and the red-wing intensity to $(C_6^e)^{0.5}$, the ~10% uncertainty in broadening translates into ~10% uncertainty in theoretical red-wing intensity. The discrepancies exceed this in most cases.

V. CONCLUSIONS

We have demonstrated that it is possible to invert quantitative collisional line-shape data which covers the line core to far wings to obtain the ground- and excited-state potentials at all R outside the close-range repulsive core. This is not a unique data-inversion process, particularly as it requires an assumed R dependence to the transition moment, but the results appear to be on very firm ground. Furthermore, these $V^*(R)$ and $V(R)$ can explain all observed features of the collisional line shape using the traditional impact and quasistatic theories combined with recent satellite-shape theories; i.e., we can explain the broadening and shift of the line core, the near wing intensity dependence, the satellite positions and distinctness, and the extreme wing intensities and temperature dependences.

The comparison of the measured near-wing intensities to the theoretical intensities for $\Delta V = -C_6^e R^{-6}$ shows qualitative but not quantitative agreement (Fig. 9). Also the C_6^* obtained from the broadening rates is not well behaved at the 30% level (Table IV). This disagreement with the theory for $\Delta V \propto R^{-6}$ can be attributed primarily to the fact that the actual long-range $\Delta V(R)$ appears to vary somewhat more slowly than R^{-6}. Often a quasistatic term also contributes to the near blue wings, as in the Tl-Xe uv line case where $\Delta V(R)$ is positive in the 4.5-Å region (Fig. 8). Thus this is not altogether a definitive test of the theory for the near-wing intensities.

---

*This work was supported in part by the Air Force Weapons Laboratory under Contract No. AFWL-75-199 and by the Advanced Research Projects Agency under Contract No. N00014-76-C-0123.

†CNRS Fellow. Present address: Laboratoire de Spectroscopie Atomique, Université de Caen, 14032 Caen Cedex, France.

‡Present address: Westinghouse Research Laboratories, Pittsburgh, Pa.

§Staff member, Laboratory Astrophysics Division, National Bureau of Standards.

[1]B. Cheron, R. Scheps, and A. Gallagher, J. Chem. Phys. 65, 326 (1976).

[2]Ch. Ottinger, R. Scheps, G. York, and A. Gallagher, Phys. Rev. A 11, 1815 (1975).

[3]R. Scheps, Ch. Ottinger, G. York, and A. Gallagher, J. Chem. Phys. 63, 2581 (1975); A. Gallagher, Phys. Rev. A 12, 133 (1975).

[4]C. J. Schuler, M. Ciftan, L. C. Bradley, III, and H. H. Stroke, J. Opt. Soc. Am. 52, 501 (1962).

[5]S. Y. Chen, M. R. Atwood, and T. H. Warnock, Physica (Utrecht) 27, 1170 (1961).

[6]H. Krefft and R. Rompe, Z. Phys. 73, 682 (1932).

[7]C. G. Carrington and A. Gallagher, Phys. Rev. A 10, 1464 (1974).

[8]K. M. Sando and J. L. Wormhoudt, Phys. Rev. A 7, 1889 (1973).

[9]After velocity-averaging Eq. (4.19) of Ref. 10, we obtain a width $\gamma(\mathrm{cm}^{-1}) = 4.43 \times 10^{-21} n(\mathrm{cm}^{-3})[T(^\circ\mathrm{K})/300\mu(\mathrm{a.m.u.})]^{0.3} C_6(\mathrm{a.u.})^{0.4}$ for $\Delta V(R) = C_6 R^{-6}$, where μ is the reduced mass.

[10]J. Szudy and W. E. Baylis, J. Quant. Spec. Radiat. Trans. 15, 641 (1975).

[11]V. V. Fomin and S. D. Tvorogov, Appl. Opt. 12, 584 (1973).

[12]S. D. Tvorogov and V. V. Fomin, Opt. Spektrosk. 30, 418 (1971) [Opt. Spectrosc. 30, 228 (1971)].

[13]T. Holstein, Phys. Rev. 79, 744 (1950), and unpublished work described in C. L. Chen and A. V. Phelps, Phys. Rev. A 7, 470 (1973).

[14]T. Proctor and W. C. Stwalley, J. Chem. Phys. (to be published).